DE GRUYTER Open Geosci. 2019; 11:901–917

Research Article

Ngo Van Liem*, Dang Van Bao, Dang Kinh Bac, Nguyen Hieu, Do Trung Hieu, Tran Van Phong, Tran Thi Viet Ha, Pham Thi Phuong Nga, and Phan Trong Trinh

Integrating Landsat 7 and 8 data to improve basalt formation classification: A case study at Buon Ma Thuot region, Central Highland, Vietnam

https://doi.org/10.1515/geo-2019-0070 Received Mar 20, 2019; accepted Oct 16, 2019

Abstract: Cenozoic basalt regions contain various natural resources that can be used for socio-economic development. Different quantitative and qualitative methods have been applied to understand the geological and geomorphological characteristics of basalt formations. Nowadays the integration of remote sensing and geographic information systems (GIS) has become a powerful method to distinguish geological formations. In this paper, authors combined satellite and fieldwork data to analyze the structure and morphology of highland geological formations in order to distinguish two main volcanic eruption episodes. Based on remote sensing analysis in this study, different spectral band ratios were generated to select the best one for basalt classification. Lastly, two spectral combinations (including band ratios 4/3, 6/2, 7/4 in Landsat 8 and 3/2, 5/1, 7/3 in Landsat 7) were chosen for the Maximum Likelihood classification. The final geological map based on the integration of Landsat 7 and 8 outcomes shows precisely the boundary of the basalt formations with the accuracy up to 93.7%. This outcome contributed significantly to the correction of geological maps. In further studies, authors suggest the integration of Landsat 7 and 8 data in geological studies and natural resource and environmental management at both local and regional scales.

Keywords: Remote sensing, geographical information system, volcanic terrain, geology, geomorphology, ratio band, Maximum Likelihood

Tran Van Phong, Phan Trong Trinh: Institute of Geological Sciences, Vietnam Academy Science and Technology, 84 Chua Lang, Hanoi, Vietnam

1 Introduction

As the largest Cenozoic basalt region in Indochina, the three main basalt eruptive episodes in Vietnam occurred respectively in the Miocene, Pliocene and Pleistocene [1, 2], with the area of more than 25,000 km² and depth of from 5 to 500 m [1, 3-5]. Cenozoic basalt regions can provide plenty of natural resources such as basalt soils for agricultural and forestry development [6, 7], bauxite sources [8, 9] and various geological heritages [10] for human well-being. Interestingly, the distribution of these three phases significantly affects land use planning and socio-economic development at both local and regional scales [9, 11-13]. However, the physical and chemical characteristics of basalt have been only analyzed at plot scales [14, 15]; while their areal distribution has been only mapped at 1: 250,000 scale in many countries [16–18], instead of at local scales because of data scarcity [19, 20].

a

In addition to traditional methods such as radiometric dating and geomorphological description [14, 15, 21], the integration between remote sensing and geographical information system (GIS) has become a potential tool to study and explain the history of geological development in volcanic regions [22-26]. Nowadays, modern sensors integrated satellites and aerial vehicles can be used freely for geological analysis at different scales, such as at national scales based on MODIS data with the low resolution from 500 m to 1 km [27] and at local/regional scales based on Sentinel-2 and unmanned aerial vehicles with the high resolution from 5 m to 10 m [28, 29]. Additionally, multispectral remote sensing bands (visible, infra-red and nearinfrared spectra) are powerful data to collect, analyze and process physical properties, soil quality and geological characteristics [30]. As spaceborne moderate-resolution data, the Landsat imageries have been applied for decades

Tran Thi Viet Ha: VNU Vietnam - Japan University, Vietnam National University, Hanoi, Vietnam

^{*}Corresponding Author: Ngo Van Liem: VNU University of Science 100000, Hanoi, Vietnam; Email: liemnv@hus.edu.vn Dang Van Bao, Dang Kinh Bac, Nguyen Hieu, Do Trung Hieu, Pham Thi Phuong Nga: VNU University of Science, Vietnam National University, Hanoi, Vietnam

in geology for interpretation of hydrothermal alteration, lithological discrimination, and tectonic setting [22, 31–34]. In order to transform spectral data to useful information/data, different innovative methods such as principal component analysis, frequency analysis, the color combination have been tested successfully in the geological and geomorphological analysis [35–38]. However, the use of the above methods to distinguish basalt phases has commonly resulted in a low accuracy in basalt rock classification.

As a solution, multiple ancillary data with texture information, such as DEM and geomorphic characteristics can be integrated with multispectral imagery to improve the basalt classification formed in the Pliocene and Pleistocene periods. Authors chose Buon Ma Thuot city in Vietnam and its surrounding region as a pilot case to investigate the potential use of Landsat 7 and Landsat 8 in the combination with GIS for basalt geological classification. Based on the remote sensing, GIS, structural, geometric and morphometric analysis and field survey data, this study aims to identify the location of volcanic eruptions, basalt distribution, and initial observations of different phases of volcanic activity. The size of basalt distribution was mapped, calibrated and standardized. Additionally, different volcanic eruptions were also interpreted. The interpretation of the origins, mechanisms and distributions of basalt soils and areas of bauxite concentration could be valuable to the geo-heritage and socioeconomic development, especially in the generation of lava caves, craters, waterfalls, lakes, columnar basalts, mines and mineral springs formed by volcanic activities [10]. The study not only has an important technical value and economic significance to improve basalt phase classification in (Central) Highland of Vietnam, but also has practical significance for mapping and editing geological maps in basalt areas.

2 Case study

The selected study region is located in the bordering areas of two provinces of Dak Lak and Dak Nong, Vietnam. The area in Dak Lak province includes Buon Ma Thuot city and part of the neighboring districts as Krong Ana, Cu Kuin, Krong Pac, Cu M'Ga and Buon Don districts. The area in Dak Nong province includes the eastern part of Cu Jut and the northeast of Krong No districts. The total research area is about 1,499 km² (Figure 1).

The highest area in the northeast part reaches about 670 m, the lowest area in the western part reaches about

200 m (Figure 1). In the southern part, the mountain ranges have been significantly divided by endogenous and exogenous processes since the Jurassic epoch. Approximately 80.4% of the study area have a slight slope (lower than 8 degrees) and only 1.4% of the area have a high slope (higher than 25 degrees) (Figure 2). In the study area, some craters and waterfalls representing cycles of tectonic activity and volcanic eruption could be observed along the Serepok river which locate in the boundary between Dak Lak and Dak Nong provinces. In the Krong No area, some lava caves recently have provided various scientific knowledge and geo-heritage values for domestic and international tourists [10].

According to a modified geological map by scientists from VNU University of Sciences based on the geological map (scale of 1:200,000) published by the Department of Geology and Minerals of Vietnam (Figure 3), the area has a relatively simple geological structure with a large area covered by Neogene-Quaternary basalt rocks belonging to the Tuc Trung formation (notated as βN_2 -Q₁tt in Figure 3) and the Xuan Loc formation (notated as Q₁²xl in Figure 3) [5]. Based on international geological classification, authors translated these two basalt formations to Pliocene (for the Tuc Trung formation) and Pleistocene (for the Xuan Loc formation) basalt formations in this study.

The Jurassic formations include three types: Dray Linh (notated as $J_1 dl$ in Figure 3), Ea Sup (notated as $J_2 es$ in Figure 3) and La Nga (notated as $J_2 ln$ in Figure 3). Quaternary sediment accumulation distributes along the river valleys, including fluvial sediments (notated as aQ_2^3 in Figure 3) and fluvial-swampy sediments (notated as aQ_2^2 in Figure 3) [8]. In order to make the basalt classification process simpler, all Jurassic formations were combined to one. The same simplification is also applied to the Quaternary sediments and then, they are called as the Quaternary formation in next sections.

Based on two field surveys in 2017 and 2018, most of residential areas in the study area are built on the Pliocene basalt formation. Because the Pliocene basalt formation distributes in flat lands with a thick weathering layer and soil of good quality, these lands are suitable for crop cultivation and residential activities. Therefore, authors included residential areas into the Pliocene basalt formation.

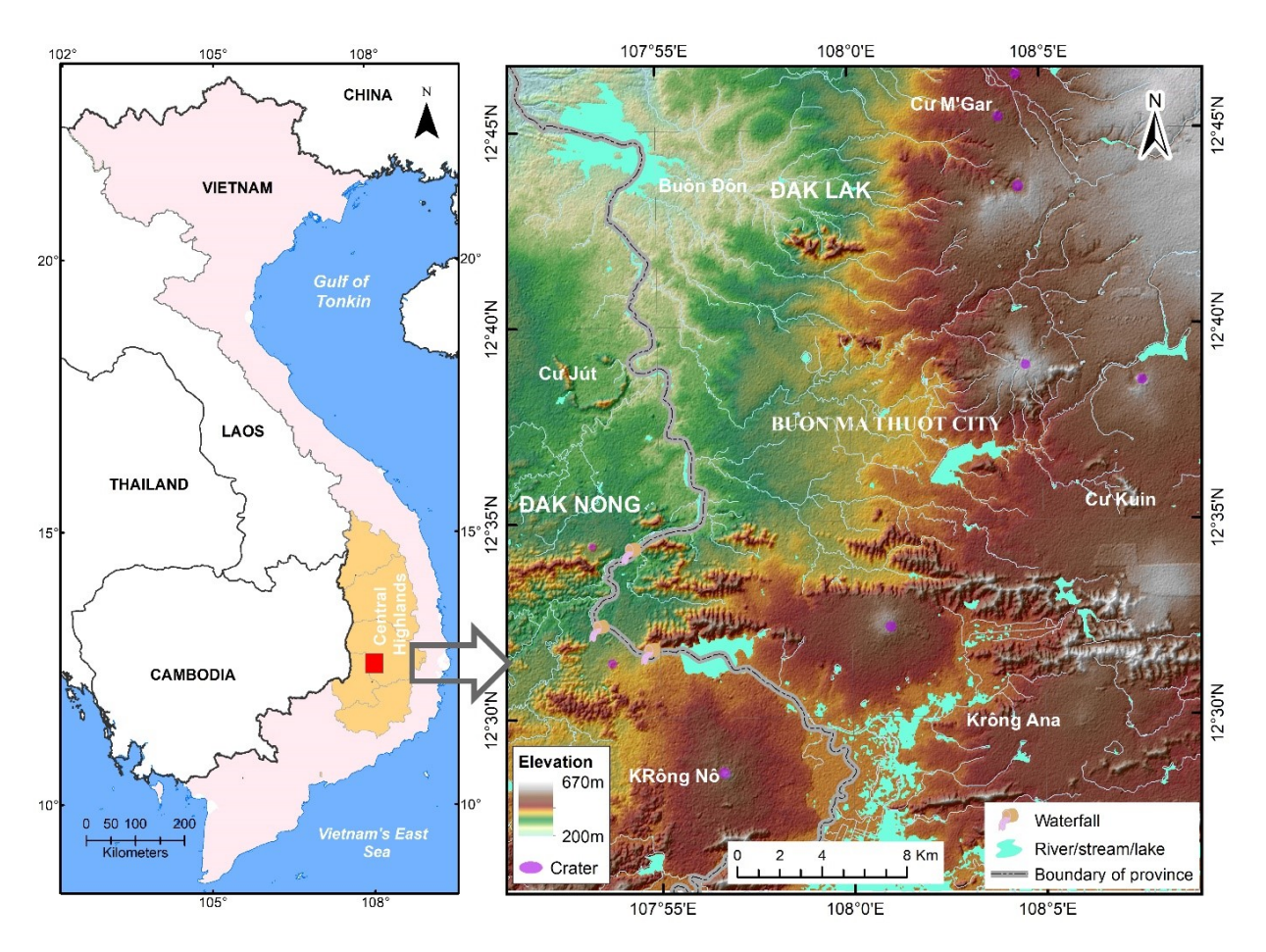


Figure 1: Location map of study area.

3 Database and methodology

3.1 Satellite selection

In order to select suitable remote sensing data for the basalt geological classification at local scales, some criterion was identified including free cost, a high number of spectral bands, available imageries taken in 2017 at medium resolution. Although ASTER and Sentinel-2 imageries provides freely a high potential to undertake semiquantitative mineral mapping, their multispectral bands have been taken in different resolutions with Landsat and not available in 2017. Whereas, Landsat imageries can be downloaded freely and updated monthly at the medium resolution of 30 m, excluding thermal infra-red band band 10 and 11 for Landsat 8, and band 6 for Landsat 7, and band 8 - Panchromatic has a resolution of 100 m, 60 m and 15 m, respectively [39, 40]. In this study, authors proposed the use of both Landsat 7 and 8 for basalt classification processes. Both Landsat generations have the same spectral ranges, therefore it is easy to compare and combine their interpretation results. The use of the Landsat 7 can improve the accuracy in the Landsat 8 interpretation and vice versa (will be presented in section 4.1). Especially, both Landsat generations are capable of providing visible, near infra-red and shortwave infra-red data (Table 1). Each spectrum captures unique energy interactions with a surface, including rock structure. Therefore, the Landsat imageries were chosen as a useful data to distinguish lithology and identifying geological structural features [41–45].

The Landsat 7 (ETM +) and Landsat 8 (OLI) satellite images used in this study were provided for free by the United States Geological Survey (USGS). Compared to the Landsat 7, sensors in the Landsat 8 were improved in performance and reliability such as 12-bit quantized image sensors that produce better image quality than 8 bits of Landsat 7. Additionally, the Landsat 8 has 11 image bands taken 250 scenes a day, whereas the Landsat 7 only has 8 image bands. In this study, the Landsat 8 (OLI) image was taken on 17/02/2017 and Landsat 7 (ETM +) image was taken on 03/03/2017. According to the Table 1, the bands of the Landsat 8 have the same wavelength and spatial resolution as

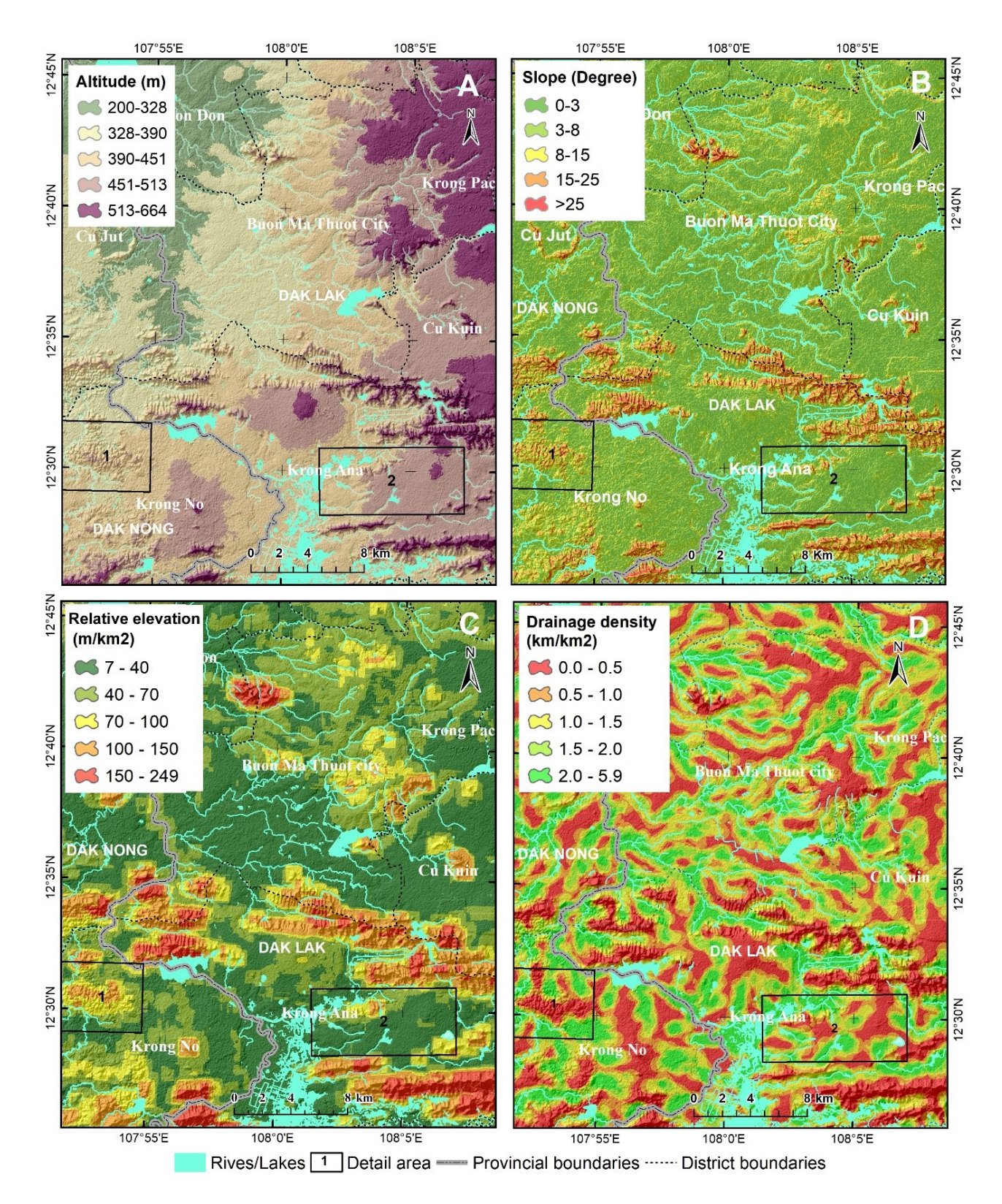


Figure 2: Morphometric maps: (a). Absolute elevation map; (b). Slope map; (c). Relative elevation map; (d). Drainage density map.

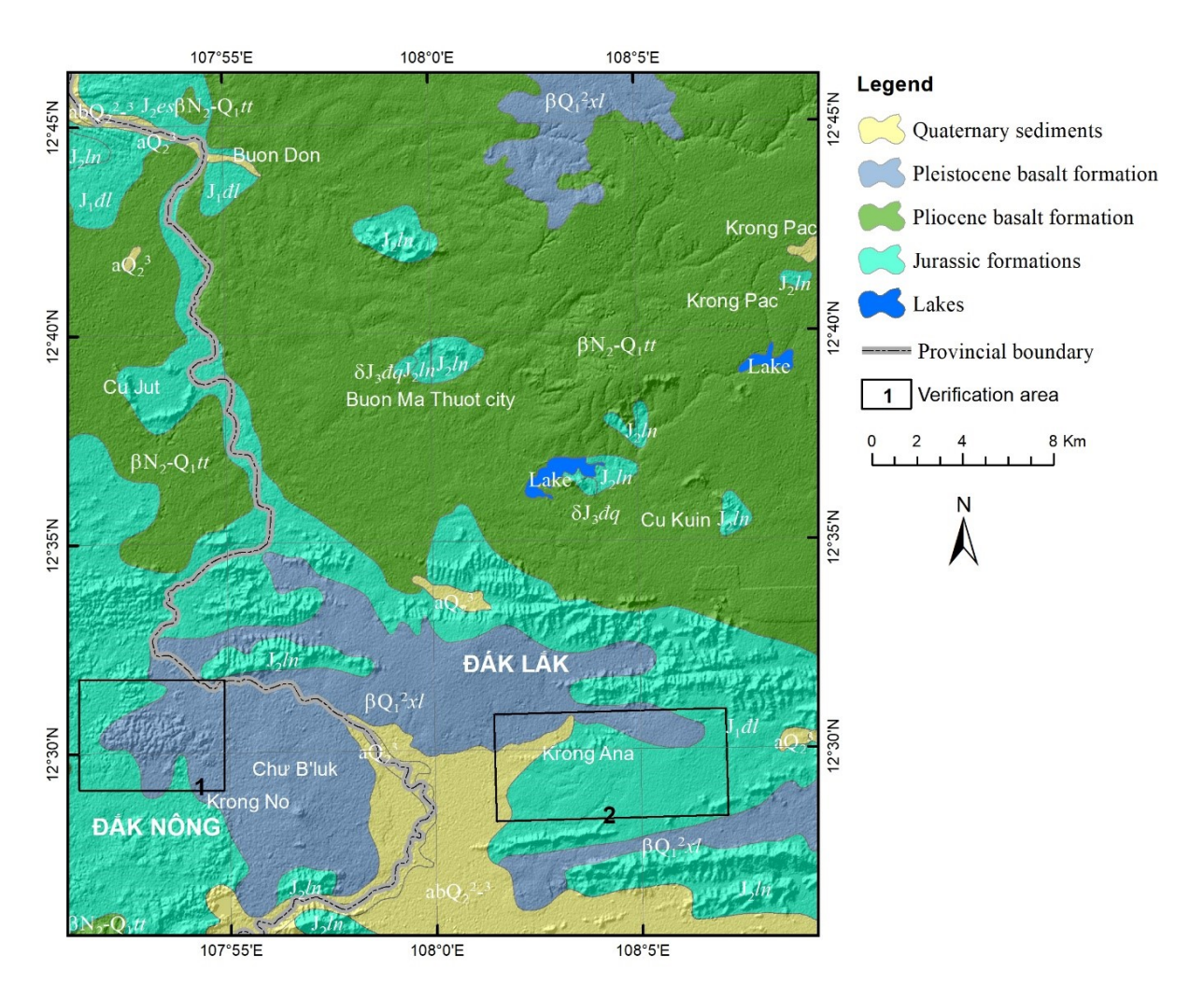


Figure 3: Geological map of Buon Ma Thuot and surrounding area (Adapted from the geological map generated by Department of Geology and Minerals.

those of the Landsat 7. The integration between results calculated from Landsat 7 and 8 is commonly used to improve the accuracy in geological analysis [29, 46–48]. The integration process will be presented in next sections.

3.2 Band ratio selection

In satellite image analysis, the band ratios have been commonly used to (1) reduce illumination effects from the sun, slope and shadows [16, 49, 50]; (2) create a new spectral band to highlight the spectral differences associated with lithological and geological structures [51]. Some popular ratios were presented in Table 2. In order to highlight the structural differences and lithological characteristics, users can produce various combinations based on band ratios generated from one Landsat satellite image taken in a particular time and place [52, 53]. The ratio selection is

necessary to distinguish main objectives with other fuzzy objectives. For instance, [52] have tested 28 color combinations based on the band ratios before selecting the best combination to identify and map the distribution of their lithological objectives in Malaysia.

In this study, authors carried out 21 different tests/combinations to select the best combination that can separate basalt phases in the study case. The visible channels for the geologic elements were selected to interpret lithological units, authors used RGB combinations between bands 6, 7 and 4 of Landsat 8 and between 5, 7 and 3 of Landsat 7 (as described in [41] as the first input ratio band for each type of the Landsat image. Additionally, the band ratios of 3 to 2; 5 to 1; and 7 to 3 of Landsat 7 and the band ratios of 4 to 3, 6 to 2 and 7 to 4 of Landsat 8 [53–57] were added to increase the contrast between lithological objectives and others as the second and third

Table 1: The spectral bands of Landsat - 8 OLI and TIRS compared to Landsat - 7 ETM+

	Landsat-7 ETM+			Landsat-8 OLI	
Spectral Band	Resolution (m)	Wavelength (µm)	Spectral Band	Resolution (m)	Wavelength (µm)
			Band 1-Coastal/Aerosol	30	0.435 -0.451
Band 1-Blue	30	0.441-0.514	Band 2-Blue	30	0.452-0.512
Band 2-Green	30	0.519-0.601	Band 3-Green	30	0.533 - 0.590
Band 3-Red	30	0.631 -0.692	Band 4-Red	30	0.636 - 0.673
Band 4-NIR	30	0.772 -0.898	Band 5-NIR	30	0.851 - 0.879
Band 5-SWIR-1	30	1.547 - 1.749	Band 6-SWIR-1	30	1.566 - 1.651
Band 6-TIR	09	10.31 - 12.36	Band 10-TIR-1	100	10.60 - 11.19
			Band 11-TIR-2	100	11.50 - 12.51
Band 7-SWIR-2	30	2.064 - 2.345	Band 7-SWIR-2	30	2.107-2.294
Band 8-Pan	15	0.515-0.896	Band 8-Pan	15	0.503 - 0.676
			Band 9-Cirrus	30	1.363 - 1.384
	(NIR-Ne	ar Infra-red; SWIR-Short Wavelen	(NIR-Near Infra-red; SWIR-Short Wavelength Infra-red; TIR-Thermal Infra-red; Pan-Panchromatic)	n-Panchromatic)	

Table 2: Summary table of lithological classification studies using band ratios

Sensor	Ratio combination	Lithology/rock	Location	References
Landsat 5 TM	5/3, 5/1, 7/5; 7/5,	Serpentinite, metavolcanics	Barramiya, Central Eastern	[48]
	5/4,3/1		Desert, Egypt	
	4/3, 5/2, 3/1; 5/3,	Limestone/marble, granite, alluvium, coastal alluvium	Dayang Bunting & Tuba	[61]
	4/3, 4/1 & 4/2, 5/3,		Islands, Langkawi, Malaysia	
	4/3			
	1/3, 5/7, 3/5; 4/5,	Granites, migmatites, gabbros, dolerites; intermediate basalts, basalts, phonolites, tuffs,	Rungwe Volcanic Province,	[62]
	6/7,4/6	phonolitic trachytes, tephraytes, sediments	Tanzania	
	3/1, 4/5, 3/2	Basaltrocks	Kula, Manisa, Turkey	[54]
Landsat 7	5/7, 5/1, 4/1	Gneisses, schists, granites; Sarabit El Khadim, Abu Hamata formations, basalt	Um Bogma, Environs	[51]
			Westcentral Sinai, Egypt.	
	3/1, 5/7, 5/4; 5/7,	Precambrian basement and the Paleozoic sedimentary rocks	Tindouf Basin (Western	[63]
	3/1,4/3		Sahara)	
	5/7, 5/1, (5/4*3/4)	Felsic and granitic rocks from mafic and ultramafic lithology of ophiolitic origin	Abidiya, Sudan	[52]
	7/3,7/2,5/2	Gossan, Marble, Diorite, Volcanic rocks	Wadi Bulghah, Saudi Arabia	[53]
	3/2, 5/1, 7/3	Volcanic rocks, acidic metamorphic (quartzite, gneiss, migmatite)	Central Region of Kenya	[44]
Landsat 8	7/5, 6/3, 6/7; 6/7,	Metamorphic rocks of volcano-sedimentary protoliths	Western Arabian Shield	[53]
	6/2 (6/5)*(4/5);			
	6/2, 7/3, 3	Ultramafic		
	6/7, 6/5, 4/2	Mafic		
	6/2, 6/7 and	Serpentine, metavolcanics	Korbiai-Gerf, SE Desert,	[32]
	(6/5)*(4/5)		Egypt	
	4/3,6/2,7/4	Neogene-Quaternary basalt, Jurassic formation, Quaternary sediment	Buon Ma Thuot, Central	Proposed in
			Highlands, Viet Nam	this study

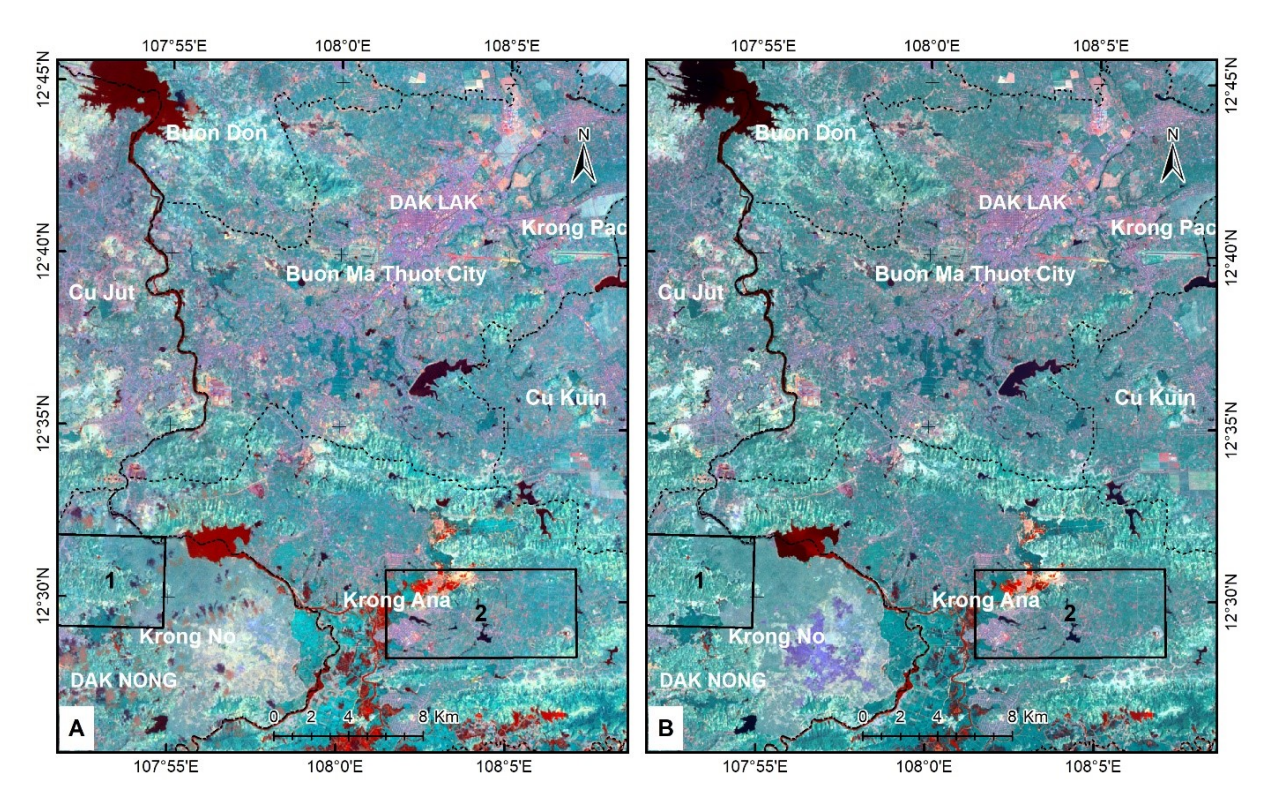


Figure 4: RGB band ratio color images: (a) Landsat 7 images (3/2, 5/1, 7/3); (b) Landsat 8 images (4/3, 6/2, 7/4).

input data for computerized interpretation (Figure 4). According to [41], these combinations can highlight major geological features such as Jurassic appears in a cyanuric color, Quaternary sediments in a blue color, and basalt formations in a lighter blue color. In this study, (satellite) imagery classification was processed by Classification tool in ENVI 5.3 software. Conversions for synchronization of the satellite imagery database, maps were made by FME Desktop 2016 software.

3.3 Additional abiotic variables

Fieldwork was conducted to study geological and geomorphological characteristics and to identify samples of different lithological types (Figure 5). Location of sample points was determined by handheld GPSMAP 78S. Accordingly, we have identified 85 sample points, including 30 basalt samples (including 19 samples from the Pliocene basalt formation and 11 samples from the Pleistocene basalt formation) and 55 other non-basalt samples (including 20 samples of Jurassic formations, 10 samples of Quaternary sedimentary formation, 10 samples of water surfaces and 15 samples of residential areas). Based on the geomorphological and hydrological characteristics of above standard samples, authors used geological map, soil map, geomor-

phological maps (slope, absolute elevation, relative elevation and river density) and satellite images to identify 228 additional samples. They include 48 samples of the Pliocene basalt formation, 36 samples of the Pleistocene basalt formation, 73 samples of Jurassic formations, 16 samples of Quaternary sediments, 27 samples of water surface and 28 samples of residential house. In total, 313 samples were collected (Figure 5) and randomly distributed at the ratio of 70% and 30% [58, 59]. Accordingly, 70% of the sample points were used for computerization (219 points), and the remaining 30% (94 points) of the samples were used to verify the results.

The Digital Elevation Model (DEM) with 12.5 m resolution was provided by the Alaska Satellite Facility (ASF), which was processed on 08/09/2009. DEM is analyzed by the Spatial Analyst Tools of ArcGIS 10.3 software. In addition, the study used satellite images, digital elevation models online provided by Google Earth Pro software. The elevation data was also added in the attribute table of sample points to compare with other remote sensing and abiotic variables.

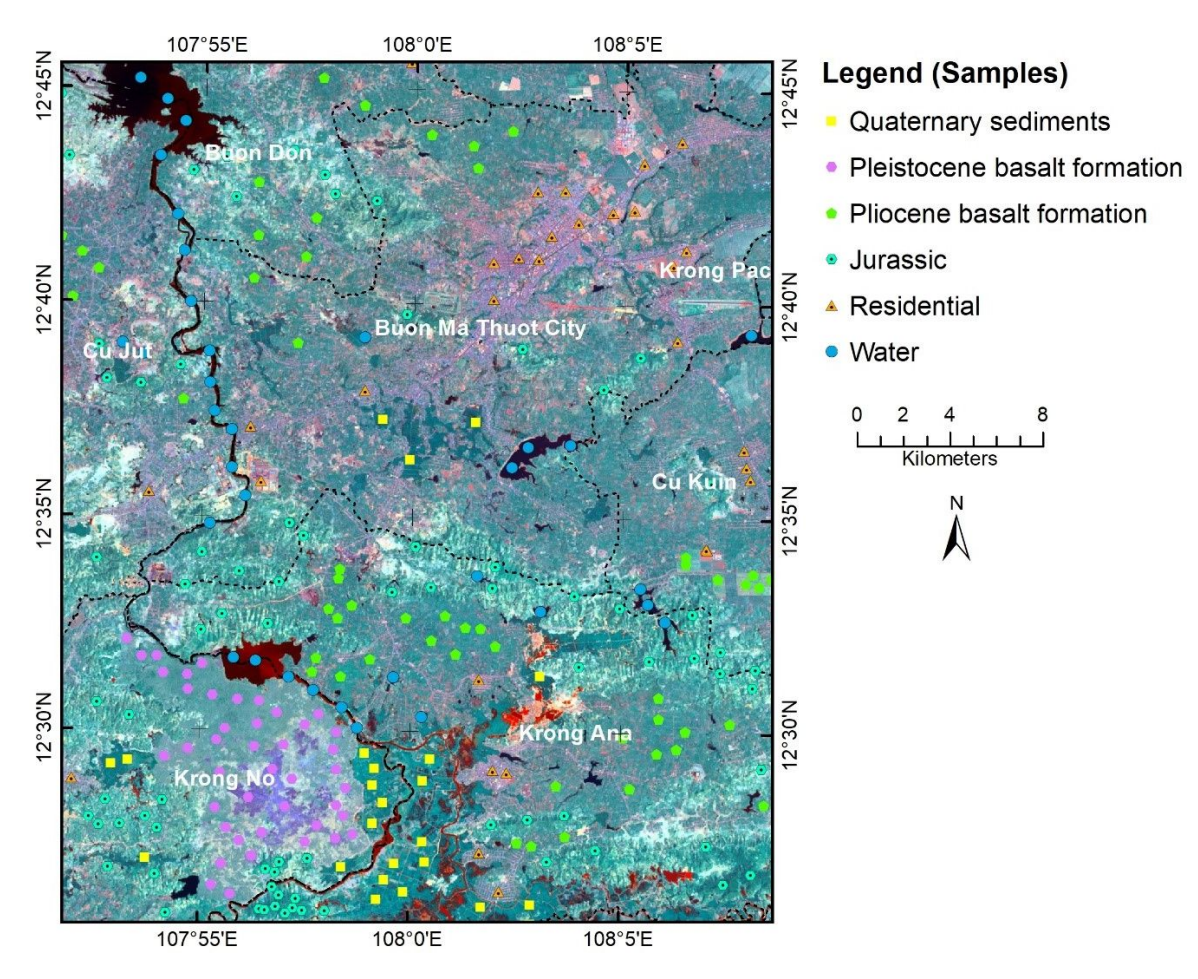


Figure 5: Distribution map of sampling points in analytical interpretation of basalt formations.

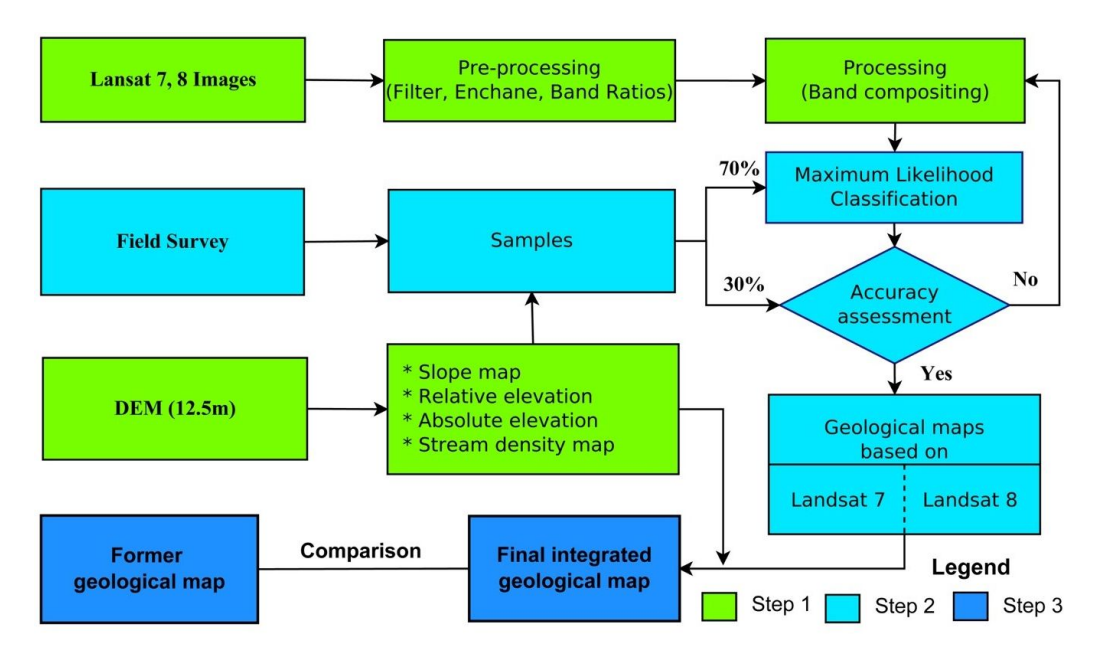


Figure 6: Flowchart of the basalt classification process. Step 1: data preparation and satellite image processing, step 2: field survey and image interpretation, and step 3: generation and validation of geological map.

3.4 Geological classification process

The flowchart of the basalt classification process is shown in Figure 6. The classification process can be divided to three steps including (1) data preparation and satellite image processing, (2) field survey and image interpretation, and (3) generation and validation of geological map. In the first step, in order to classify the lithology in Buon Ma Thuot and neighboring areas, Landsat 7 and 8 satellite images which were compositing in RGB by the band ratios. Band ratios are obtained easily by dividing digital number of each pixel at the one location in one band by each pixel at the same location in another band. Thus, band ratio technique highlights the spectral differences related to the specific materials to be mapped and disintegrates these surface materials from each other; otherwise, such information will not be available in any single band [57]. By applying this technique, lithology structures can be best distinguished by a combination of ratios that include short wavelength bands, the ratio of the long wavelength bands, and a ratio of one band each from short and long wavelength band groups [51].

The RGB band ratio combination will be categorized according to the supervised classification. This is a probabilistic method that is able to arrange user-defined pixels into different classes. In it, all the pixels in an image are identified by the same spectral notation for the purpose of recognizing the identity, representative samples representing the different expressions that we want to classify. Standard samples were usually selected directly in the field or rely on reliable sources such as aerial photographs, satellite images and related maps. Accordingly, the more samples selected, the more accurate the classification will be. The sampling sites used a spectrum to give an outline of those areas. Digital image classification used spectrum information represented by one or more spectral channels of satellite imagery and attempts to classify each pixel independently based on this spectral information. In other cases, the objects are assigned all the pixels in the image according to the individual layers or the individual threads.

Supervised classification techniques include parallelepiped, minimum distance, maximum likelihood, spectral angle mapper (SAM), spectral information divergence (SID), and binary encoding. The most commonly used classification methods are the maximum likelihood classification (MLC) [60–62]. The MLC considers the statistics of each class in each image band to be dispersed in a regular manner and this method considers the ability of a pixel of a given class. Without selecting a probability threshold, all pixels must be sorted. Each pixel is assigned to a class

with the highest probability (*i.e.*, "Maximum likelihood"). This method is based on the hypothesis that the probability density function for each class is multivariate, and an unknown pixel is assigned to a class with the highest probability of belonging [62, 63]. The calculation is based not only on the distance value, but also on the degree of gray variation in each layer. This is an accurate classification method but takes a lot of time to compute and depends on the standard distribution of the data (as described by [60] for more detail).

In the second step of the flowchart of the basalt classification process, four geomorphological factors generated based on DEM at resolution 12.5 m include slope, relative elevation and absolute elevation and drainage density. The geomorphological characteristics were assigned to 313 samples that were collected in section 3.3.75% of data were separated to be used as training data, whereas the rest of data were used as testing data to interpreted geological maps based on Landsat image in step 2. The distribution of geological samples will be validated in four above geomorphological factors. This information is important to classify geological classes in step 3 with the integration with outcomes from step 1. In step 3, the last field survey was carried out in October 2018 to validate the location of the Quaternary basalt formations, especially based on the appearance of craters. The main outcome is presented in section 4.3.

4 Results

4.1 Geological maps based on Landsat 7 and 8 analysis

Using the maximum likelihood classification method and carrying out the steps of the research process as described above, geological maps was developed based on the Landsat 7 and 8 data as shown in Figure 7. The lithological structures interpreted from the Landsat 7 data shows a more homogeneous distribution of the Pliocene basalt formation in Buon Ma Thuot city, Krong No and Krong Ana districts compared to outcomes from the Landsat 8 data. The contrast outcomes were found with the Pleistocene basalt formation. This formation distributes heterogeneously in the geological map based on the Landsat 7 and homogeneously in the map based on the Landsat 8. Both maps show that most area in Buon Ma Thuot city were formed on Pliocene basalt formation. The vestiges of the Quaternary formation were detected along the boundary of Krong No and Krong Ana districts. The Jurassic formation could be

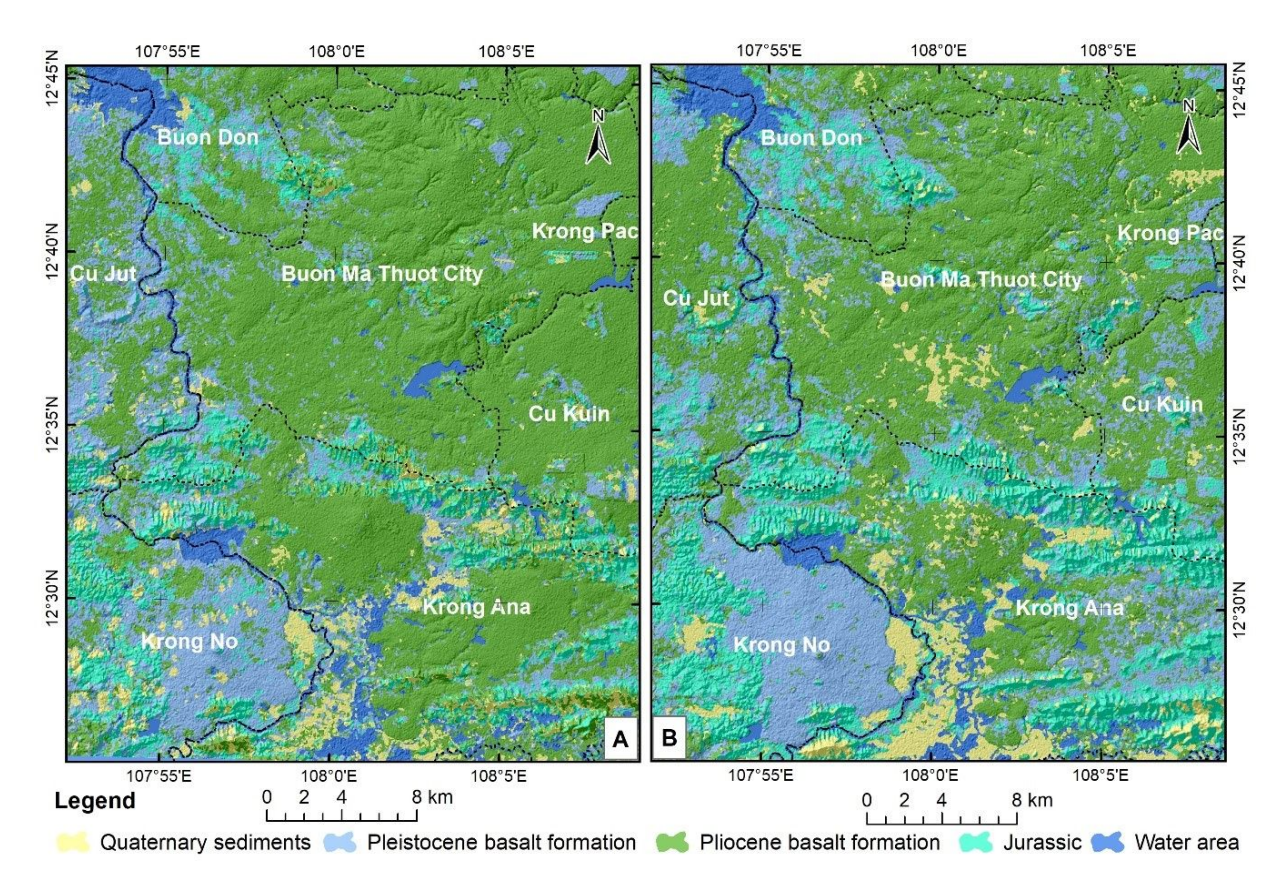


Figure 7: Geological maps generated based on Landsat 7 (A) and 8 (B) data.

Table 3: Areal distribution of geological formations based on geological maps generated from Landsat 8 and Landsat 7 data at Buon Ma Thuot city and surrounding areas

No.	Objects of interpretation	Based on Landsat 8 data		Based on Landsat 7 data	
		Area (ha)	Percentage (%)	Area (ha)	Percentage (%)
1	Quaternary sedimentary	9534.1	6.4	8396.1	5.6
2	Basalt Pleistocene formation	32340.2	21.6	28936.7	19.3
3	Basalt Pliocene formation	72936.5	48.6	82911.8	55.3
4	Jurassic formation	27093.2	18.1	21590.1	14.4
5	Water surface formation	8027.2	5.3	8096.3	5.4
	Total	149931.0	100	149931.0	100

found in mountainous areas along the boundary of Krong Ana district and Buon Ma Thuat city.

The areal distribution and percentage of geological formations in the study case were shown in the Table 3. According to the percentage of all formations, the Pliocene basalt formation takes more than 55% of the whole region. The Pleistocene and Jurassic formations take from 14 to 19% of the whole region. The obvious difference between the outcomes from Landsat 7 and 8 data could be detected in Jurassic, Pleistocene and Pliocene basalt formations. The area of the Pleistocene basalt and Jurassic formations based on the Landsat 8 data is 3,000 ha and 6,500

ha respectively larger than those based on the Landsat 7 data. By contrast, the Pliocene basalt formation found in Landsat 8 is 10,000 ha smaller than in Landsat 8. The areal distribution of other formations in both data were similar.

The accuracy of the results is shown in Tables 4 and 5. By using 30% of the remaining sample points (94 sample points) overlap the result map and count, it can be concluded that the accuracy of using Landsat 8 images was higher (89.9%) than using Landsat 7 images (80.3%). Interestingly, the Quaternary sedimentary samples were identified correctly 100%, whereas other formations were predicted with the accuracy of from 80 to 87% in both Landsat

Table 4: Evaluate accuracy in interpretation of objects using Landsat 8 images

No.	Objects	Total of samples	Corrected samples	Uncorrected samples	Accuracy (%)	Errors (%)
			· · · · · · · · · · · · · · · · · · ·	Jumpics		
1	Pliocene formation	32	26	6	81.3	18.8
2	Pleistocene formation	12	12	0	100.0	0.0
3	Jurassic formation	31	25	6	80.6	19.4
4	Quaternary sedimentary	11	11	0	100.0	0.0
5	Water surface	8	7	1	87.5	12.5
	Total/Average	94	81	13	89.9	10.1

Table 5: Evaluate accuracy in interpretation of objects using Landsat 7 images

No.	Objects	Total of samples	Corrected samples	Uncorrected samples	Accuracy (%)	Errors (%)
1	Pliocene formation	32	30	2	93.8	6.3
2	Pleistocene formation	12	4	6	33.3	66.7
3	Jurassic formation	31	27	4	87.1	12.9
4	Quaternary sedimentary	11	11	0	100.0	0.0
5	Water surface	8	7	1	87.5	12.5
	Total/Average	94	79	13	80.3	19.7

data. The total accuracy of the outcomes based on Landsat 7 data was reduced, especially in the Pleistocene basalt formation on the one hand when the accuracy of this formation only reached 33%. Compared to the outcomes based on the Landsat 8, the Pliocene basalt formation detected from Landsat 7 is better than 10%.

4.2 Geomorphological characteristics of basalt formations

Figure 8 showed the distribution of geological formations in different geomorphological and hydro- factors. Three basalt formations distribute at the elevation of from 400 to 500 m, whereas the Jurassic formation distribute in a wider range of elevation. The Quaternary basalt formation distribute mostly on about 400 m elevation. It is easier to observe differences between three basalt formations, as well as with the Jurassic formation, based on the relative elevation. The younger geological formations (such as the Quaternary basalt formation) have a lower value of relative elevation, compared to older ones (such as the Pliocene basalt formation). The similar trend is also found in the figure showing the distribution of basalt formation in different slope levels. The river density in four geological formations (including Jurassic one) seems to be more complex. The higher river density can be found in the Quaternary basalt formation, following to the Pliocene basalt formation. The older geological formations (such as the Jurassic and Pleistocene formations) have lower river density.

4.3 Final geological map based on the integration of Landsat 7 and 8 data

After validating the interpretation results of two Landsat data, the final geological map of the study case was carried out with the expert analysis in field surveys, topographical data, and associated maps. The boundaries of the major geological formations were delineated in the study area. Accordingly, the study area was divided into three main geological groups: basalt, Jurassic and Quaternary formations. Particularly, the basalt formation was divided into two specific types: Pliocene basalt and Pleistocene basalt formation. Especially, the classification between basalt and non-basalt formations shown in the Figure 9 is the integration of two interpretation results. Whereas the boundary of Pleistocene basalt formation was inherited from the Landsat 8 interpretation result (with accuracy of 100%), the boundary of Pliocene basalt formation was inherited from the Landsat 7 interpretation result (with accuracy of 93.8%) (Table 6). Therefore, the average accuracy of basalt geological classification based on Landsat data would be 96.9% and of all five geological formations would be 93.7%. As another result, eight ancient craters were identified and six of them locate in the Pliocene basalt formation.

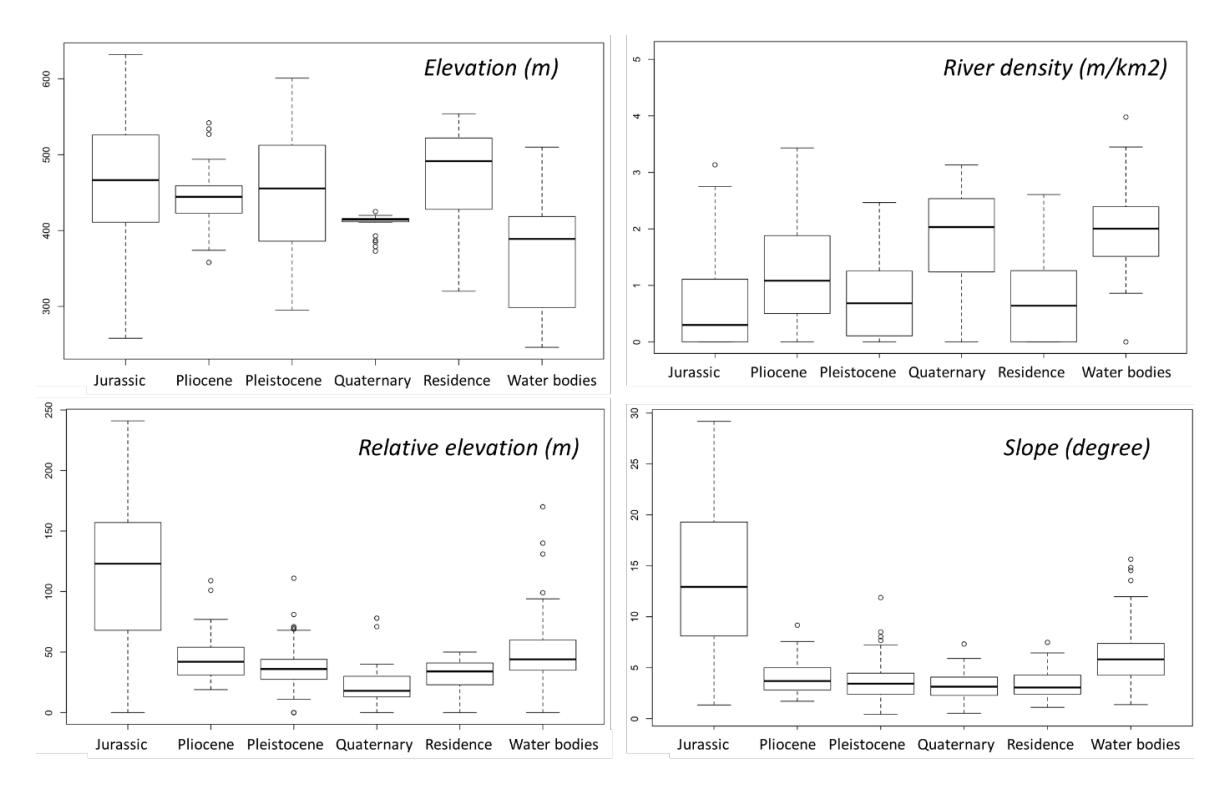


Figure 8: Distribution of basalt formations in different geomorphological and hydro-characteristics.

Table 6: Accuracy comparison between three interpretation results

No.	Objects	Accuracy of geological map based on (%)					
		Landsat 8	Landsat 7	Integration of Landsat 7 and 8			
1	Pliocene formation	81.3	93.8	93.8			
2	Pleistocene formation	100.0	33.3	100.0			
3	Jurassic formation	80.6	87.1	87.1			
4	Quaternary sedimentary	100.0	100.0	100.0			
5	Water surface	87.5	87.5	87.5			
	Total/Average	89.9	80.3	93.68			

It is easy to observe the large area of the Buon Ma Thuot city and Cu Kuin, Krong Ana and Cu Jut districts have been formed on the Pliocene basalt formation. Whereas, the Krong No district is mainly formed on the Pleistocene basalt formation. The Jurassic formation distribute heterogeneously among other formations.

5 Discussions

5.1 Potential use of spectral band ratios in other geological studies

The interpretation results based on Landsat 7 and 8 for geological classification proved the potential of spectral

band ratios as mentioned in previous geological studies that only used one type of data [36, 52, 53]. The interpretation for a single satellite image can commonly distinguish main geological formations such as Jurassic, Neogene and Quaternary formations but this method could not separate different geological materials in detail in each formation. The integration between two Landsat generations has taken full advantage of each interpretation result, particularly in basalt classification. In the case of research area, while the use of Landsat 7 data can interpret basalt materials belong to the Pliocene basalt formation, the use of Landsat 8 data can interpret basalt materials belong to the Pleistocene basalt formation. Therefore, authors propose the use of single satellite data for geological classification in general as the first step, and the use of integrated

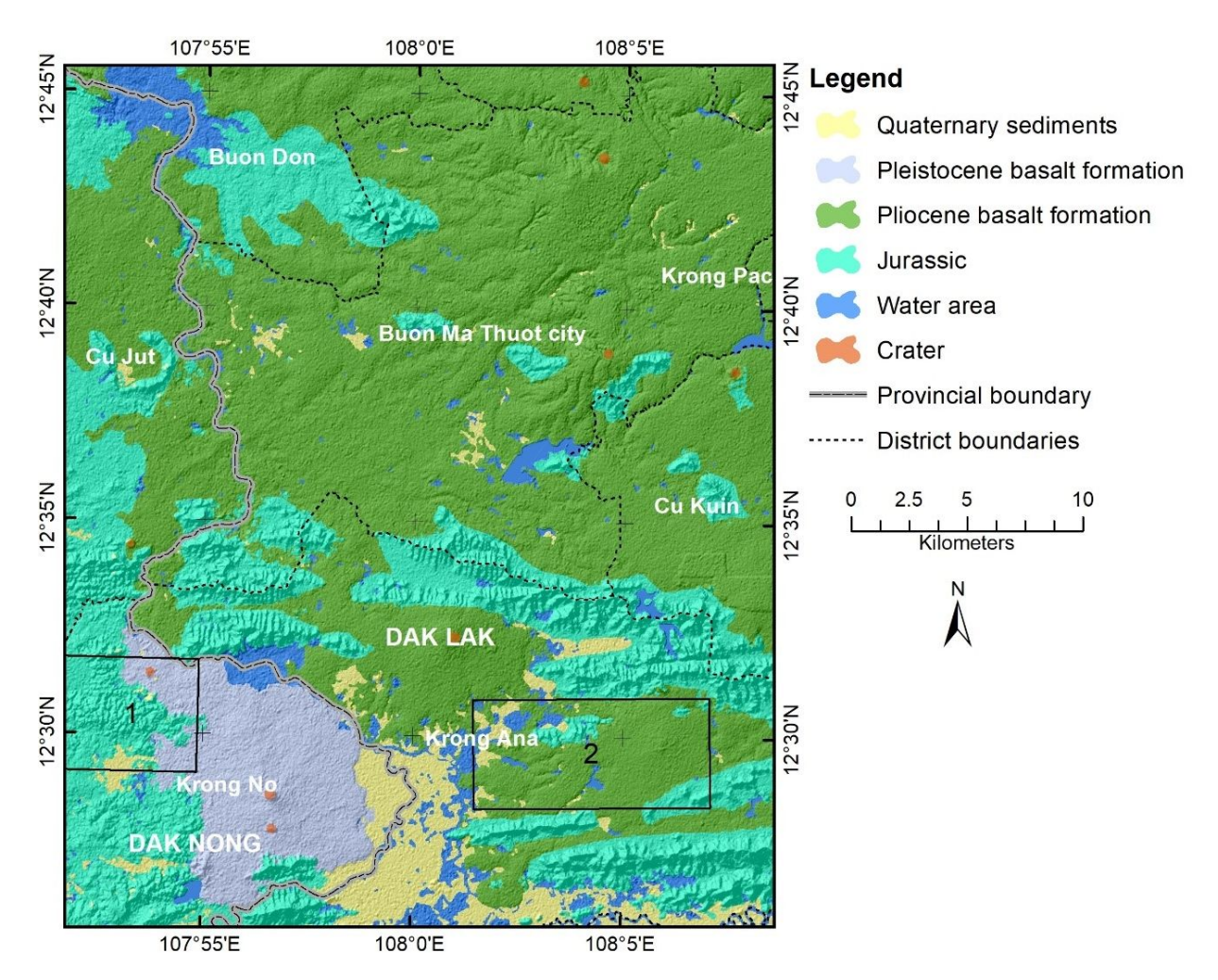


Figure 9: The geological map based on integration of Landsat 7 and 8.

satellite data for basalt geological classification in detail. The successful development of new spectral band ratios for Landsat satellite images to classify basalt formations have proved a high potential use of these ratios for other satellite images such as Aster and Sentinel-2 images.

5.2 Comparison of the results with the traditional geological maps

Compared to the formal geological maps (at 1: 200,000 scale) published by the Department of Geology and Minerals of Vietnam (Figure 3), some differences between geological formations can be found as following:

The **first** issue relates to the accuracy of basalt and non-basalt formations based on the analysis of both morphological features and remote sensing. The Jurassic formation has made a complex terrain with high slope, deep division (Figures 2b and 2c) and a small drainage density (Figure 2d). Based on both Landsat satellite images, the

Jurassic formation can be characterized with cyan color and rough structures, while the Quaternary formation can be identified with dark blue and smooth structure (Figure 4). However, the identification of basalt and non-basalt boundaries are different in the interpretation results with geological map (Figure 3).

In this section, authors emphasize two specific cases, such as in black frames that were denoted as "1" and "2" in Figures 4 and 8. In the frame 1, the Pleistocene basalt formation in the geological map (Figure 3) is overlapped the Jurassic formation. In fact, some lava caves were only found in the north-eastern sides of these overlapping areas, whereas a complex terrain formed by Jurassic formation could be observed easily in the western side of the frame 1 on the one hand. The distinguishing of the Jurassic and Pleistocene basalt formations in the frame 1 has proved the high accuracy of interpretation results. Another result was found in the frame 2. The satellite image showed a darker blue and finer texture of the Pliocene

914 — N. Van Liem et al. DE GRUYTER

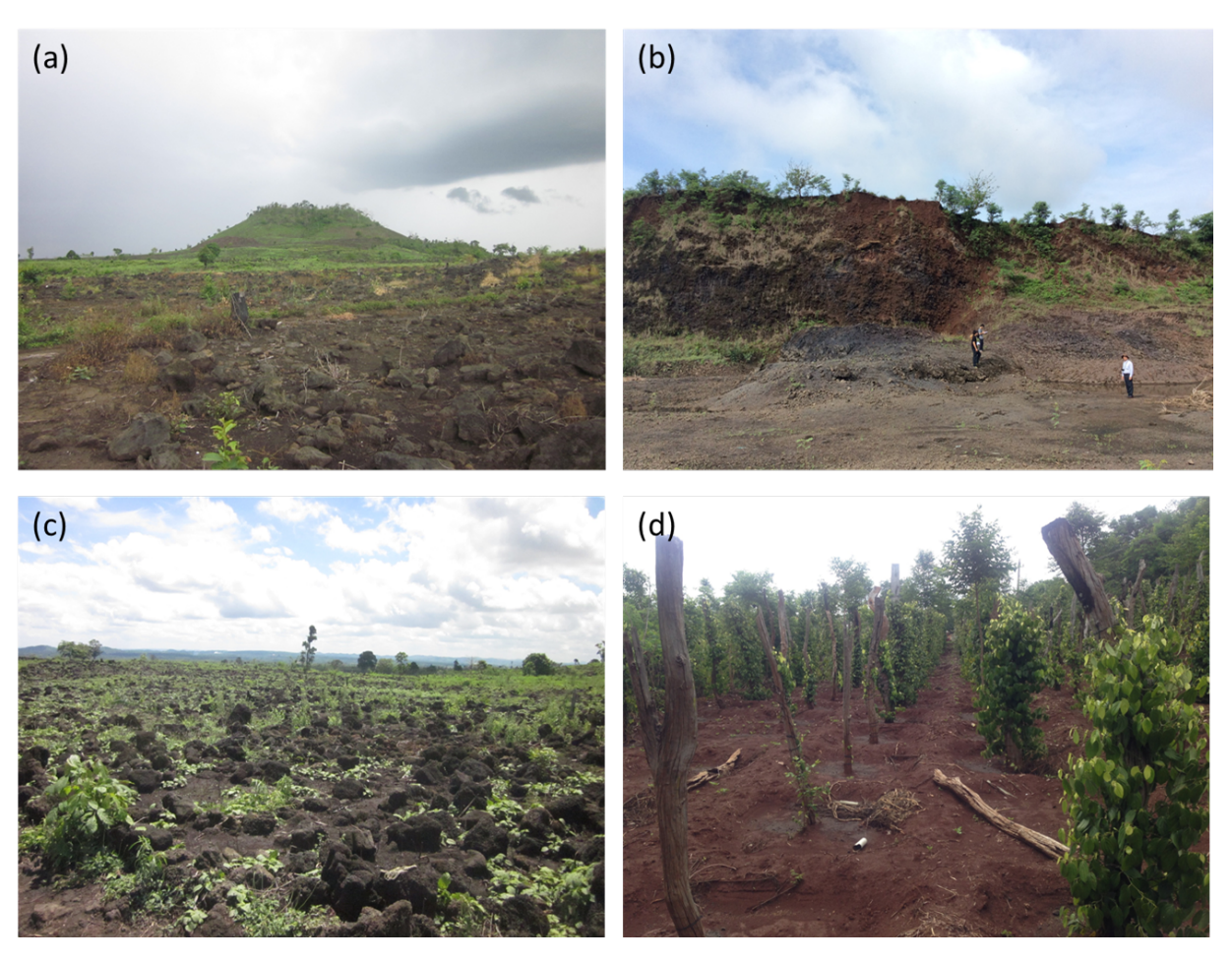


Figure 10: Basalt at (a) Pleistocene formation in Chu B'luk volcano area, Krong No district, Dak Nong; (b) Pliocene formation, in Buon Ma Thuot city, Dak Lak; (c) in Chu B'luk, Krong No area; and (d) in Buon Ma Thuot City.

basalt tone and morphological maps (Figure 2b and 2c) showed that this area was characterized by small slopes and deep divisions like the Pliocene basalt formation. However, the area in the frame 2 was identified as the Jurassic formation in the geological map. Thus, the correct realignment between the basalt and non-basalt formations in the area of this result is very significant in correcting and re-normalizing the types of geological maps at the average scales (*e.g.* 1: 200,000 to 1: 50,000).

According to the geological map (Figure 3), the Pleistocene basalt formation **secondly** accounted for a major area of the Krong Ana district and a part of the Buon Ma Thuot city, while this formation was not found at the same places in the interpretation result (Figure 9). In Figure 4b, the spectrum of the Pleistocene basalt formation in the Krong No area are lighter green and brighter compared to the rest of the study area. In fact, the Pleistocene basalt rocks in Krong No district is relatively fresh, with poor weathering (Figure 10a and 10c), while the Pliocene basalt

are strongly weathered, creating a thick basalt soil in other areas (Figure 10b and 10d).

Lava caves, as another method to identify the area of the Pleistocene basalt formation, were found not only in Krong No district, but also in the Central Highlands of Vietnam. The location of these caves was found in the boundary of the Pleistocene basalt formation in the interpretation results. Although [5, 10, 13] also found the lava caves in Tan Phu and Dinh Quan area, Dong Nai province - Southeast Vietnam, he did not identify the geological formation of these caves. It is possible that basalt caves are formed only in the youngest geological period, so they are well preserved until today. Additionally, the distribution of "Quaternary basalt formation" in the interpreted maps was validated firstly based on the appearance of lava tubes' mouths. In other words, the accuracy of outcomes to interpret the "Quaternary basalt formation" is high. Secondly, the outcomes (geological maps) were interpreted at the regional scale can become more useful for studies at the plot

scales, especially in the identification of unknown lava tubes' mouths by many interdisciplinary scientists.

6 Conclusions

The study presented the analysis and interpretation processes of satellite imageries in combination with the digital elevation model and morphometric maps to classify the geological formations and to identify the ancient craters in a highland area, Vietnam. Three main issues can be concluded as following:

- Based on medium resolution data of the Landsat 7 and 8 satellite images, the lithological and volcanic landform features can be identified with a high accuracy at both regional and national scales, especially with the basalt area of Pleistocene basalt and Pliocene basalt formations.
- The boundary of geological formations (e.g. basalt and non-basalt distribution) or geological maps obtained from Landsat data can be a used to calibrate/validate traditional geological maps and to interpret different volcanic eruptions and caves.
- The integration of Landsat 7 and 8 data can be a powerful tool not only for geological studies, but it also provides various information for natural resource and environmental management.

Acknowledgement: This study was supported by Vietnam National University, Hanoi, project code QG.17.23. We are thankful to the VNU University of Science, Vietnam National University, Hanoi for providing all the facilities for this research. We are grateful for the time and efforts from the editors and the anonymous reviewers on improving our manuscript.

References

- Hoang N, Flower M, Chi C, Xuan P, Quy H, Son T, Collision-induced basalt eruptions at Pleiku and Buon Me Thuot, south-central Viet Nam. J Geodyn, 2013, 69, 65–83,
- [2] Xuan P, Hoang N, Koo L, Geochemistry of late Cenozoic basalts in Vietnam and its tectonic significances. J Geol, 2004, 24B,
- [3] Anh L, Thuy N, Thanh N, Nam H, Assessment of organic matter content in basalt soils under cultivation of major crops in Dak Lak province. Vietnam J Earth Sci, 2015, 37, 110–7, (in Vietnamese with English summary)
- [4] Dung T, Minh N, Eruptive-volcanic-basalt structures in the Truong Sa-Spratly Islands and adjacent areas from interpreting gravity and magnetic data. Vietnam J Earth Sci, 2017, 39, 1–13,

- [5] Hoang N, Shinjo R, Phuc LT, Anh LD, Huong TT, Pécskay Z, et al., Pleistocene basaltic volcanism in the Krông Nô area and vicinity, Dac Nong Province (Vietnam). J Asian Earth Sci, 2019, 181 (January), 103903, https://doi.org/10.1016/j.jseaes.2019. 103903
- [6] Zhou Y, Retallack GJ, Huang C, Early Eocene paleosol developed from basalt in southeastern Australia: implications for paleoclimate. Arab J Geosci, 2014, , 13,
- [7] Vingiani S, Terribile F, Meunier A, Petit S, Catena Weathering of basaltic pebbles in a red soil from Sardinia: A microsite approach for the identi fi cation of secondary mineral phases. Catena, 2010, 83 (2-3), 96-106, http://dx.doi.org/10.1016/j.catena.2010.07. 001
- [8] Dao N, Yem N, Tuyet N, Tam L, Geomorphological features of the basalt areas in the South Vietnam. J Geol, 1986, 172 (1), 17–20, (in Vietnamese with English summary)
- [9] Nien B, Anh T, Dung P, Hieu T, Ly V, Mai N, et al., Overview of precious stones, half precious stones, fine arting stones, ashlar facing stones and potentiality of them in the Tay Nguyen zone. Vietnam J Earth Sci, 2015, 37, 16–27, (in Vietnamese with English summary)
- [10] Phuc L, Tachihara H, Honda T, Tuat L, Thom B, Hoang N, Chikano Y, Yoshida, K, Tung N, Danh P, Hung M, Duc T, Vu P, Hoa N, Bien H, Quy T, Minh N,. Geological values of lava caves in Krongno Volcano Geopark, Dak Nong, Vietnam. Vietnam J Earth Sci, 2018, 40(4), 299-319,
- [11] Ha N, Dung N, Ngoc H, Application of USLE and GIS tool to predict soil erosion potential and proposal land cover solutions to reduce soil loss in Tay Nguyen. Vietnam J Earth Sci, 2013, (35), 403–10, (in Vietnamese with English summary)
- [12] Phuong TH, Hai TQ, Bao D Van, Some natural heritages of outstanding values for tourism development in Central Highland. Vietnam J Earth Sci, 2015, 37 (2), http://dx.doi.org/10.15625/ 0866-7187/37/2/7375
- [13] Phuc LT, Su NK, Duc VT, Tuat LT, Toan PT, Tung NT, et al., New discovery of prehistoric archaeological remnants in volcanic caves in K'Rongno, Dak Nong province. Vietnam J Earth Sci, 2017, 39 (2), http://dx.doi.org/10.15625/0866-7187/39/2/9186
- [14] Monaldo E, Nerilli F, Vairo G, Basalt-based fiber-reinforced materials and structural applications in civil engineering. Compos Struct, 2019, 214, 246-63, https://doi.org/10.1016/j.compstruct.2019.02.002
- [15] Monaldo E, Nerilli F, Vairo G, Effectiveness of some technical standards for debonding analysis in FRP-concrete systems. Compos Part B Eng, 2019, 160, 254–67, https://doi.org/10.1016/j. compositesb.2018.10.022
- [16] Sultan M, Arvidson RE, Sturchio NC, Guinness EA, Lithologic mapping in arid regions with Landsat thematic mapper data: Meatiq dome, Egypt. Geol Soc Am Bull, 1987, 99 (6), 748, http://dx.doi.org/10.1130/0016-7606(1987)99%3C748:lmiarw %3E2.0.co
- [17] Tran, Nguyen, Geological Map of Vietnam 1:1500000. 1986,
- [18] Msindai KA, Engineering geological mapping of Dar es Salaam city, Tanzania. Tanzania J Sci, 2004, 28 (2), http://dx.doi.org/10. 4314/tjs.v28i2.18356
- [19] Anh LD, Hoang N, Shakirov RB, Huong TT, Geochemistry of late miocene-pleistocene basalts in the Phu Quy island area (East Vietnam Sea): Implication for mantle source feature and melt generation. Vietnam J Earth Sci, 2017, 39 (3), http://dx.doi.org/ 10.15625/0866-7187/39/3/10559

- [20] Dung TT, Minh NQ, Eruptive-volcanic-basalt structures in the Truong Sa-Spratly Islands and adjacent areas from interpreting gravity and magnetic data. Vietnam J Earth Sci, 2017, 39 (1), http: //dx.doi.org/10.15625/0866-7187/39/1/9167
- [21] Borrelli L, Antronico L, Gullà G, Sorriso-Valvo GM, Geology, geomorphology and dynamics of the 15 February 2010 Maierato landslide (Calabria, Italy). Geomorphology, 2014, 208 (February 2010), 50-73, http://dx.doi.org/10.1016/j.geomorph.2013. 11.015
- [22] Kervyn M, Kervyn F, Goossens R, Rowland SK, Ernst GGJ, Mapping volcanic terrain using high-resolution and 3D satellite remote sensing. Geol Soc, 2007, , 5-30,
- [23] Merrett HC, Chen WW, Applications of geographical information systems and remote sensing in natural disaster hazard assessment and mitigation in Taiwan. Geomatics, Nat Hazards Risk, 2013, 4 (2), 145-63, http://dx.doi.org/10.1080/19475705.2012.
- [24] Pande CB, Khadri SFR, Moharir KN, Patode RS, Assessment of groundwater potential zonation of Mahesh River basin Akola and Buldhana districts, Maharashtra, India using remote sensing and GIS techniques. Sustain Water Resour Manag, 2017, 4 (4), 965-79, http://dx.doi.org/10.1007/s40899-017-0193-5
- [25] Mwaniki M, Möller M, Mwaniki MW, Matthias MSM, Schellmann G, Application of Remote Sensing Technologies to Map the Structural Geology of Central Region of. 2015, (March),
- [26] Liem N Van. Dat NP. Dieu BT. Phai V Van. Trinh PT. Vinh HO. et al., Assessment of Geomorphic Processes and Active Tectonics in Con Voi Mountain Range Area (Northern Vietnam) Using the Hypsometric Curve Analysis Method. Vietnam J Earth Sci, 2016, 38 (2), http://vjs.ac.vn/index.php/jse/article/view/8602
- [27] Ganguly S, Nemani RR, Zhang G, Hashimoto H, Milesi C, Michaelis A. et al., Generating global Leaf Area Index from Landsat: Algorithm formulation and demonstration. Remote Sens Environ, 2012, 122, 185-202, http://www.sciencedirect.com/ science/article/pii/S0034425712000442
- [28] van der Meer FD, van der Werff HMA, van Ruitenbeek FJA, Potential of ESA's Sentinel-2 for geological applications. Remote Sens Environ, 2014, 148, 124-33, http://dx.doi.org/10.1016/j. rse.2014.03.022
- [29] Mandanici E, Bitelli G, Preliminary Comparison of Sentinel-2 and Landsat 8 Imagery for a Combined Use. Remote Sens, 2016, 8 (12), 1014, http://dx.doi.org/10.3390/rs8121014
- [30] Abdelrahman MAE, Natarajan A, Hegde R, Assessment of land suitability and capability by integrating remote sensing and GIS for agriculture in Chamarajanagar district, Karnataka, India. Egypt J Remote Sens Sp Sci, 2016, 19 (1), 125-41, http: //dx.doi.org/10.1016/j.ejrs.2016.02.001
- [31] Thouret J-C, Volcanic geomorphology—an overview. Earth-Science Rev, 1999, 47 (1-2), 95-131, http://dx.doi.org/10.1016/ s0012-8252(99)00014-8
- [32] Moore CA, Hoffmann GA, Glenn NF, Quantifying Basalt Rock Outcrops in NRCS Soil Map Units Using Landsat-5 Data. Soil Horizons, 2007, 48 (3), 59, http://dx.doi.org/10.2136/sh2007.3.0059
- [33] Prima ODA, Yoshida T, Characterization of volcanic geomorphology and geology by slope and topographic openness. Geomorphology, 2010, 118 (1-2), 22-32, http://dx.doi.org/10.1016/j. geomorph.2009.12.005
- [34] Mitchell JJ, Shrestha R, Moore-ellison CA, Glenn NF, Single and Multi-Date Landsat Classifications of Basalt to Support Soil Survey Efforts. 2013, (December 2014),

- [35] Behnia P, Harris JR, Rainbird RH, Williamson MC, Sheshpari M. Remote predictive mapping of bedrock geology using image classification of Landsat and SPOT data, western Minto Inlier, Victoria Island, Northwest Territories, Canada. Int J Remote Sens, 2012, 33 (21), 6876-903, http://dx.doi.org/10.1080/01431161. 2012.693219
- [36] Leverington DW, Moon WM, Landsat-TM-Based Discrimination of Lithological Units Associated with the Purtuniq Ophiolite, Quebec, Canada. Remote Sens, 2012, 4 (5), 1208-31, http://dx.doi. org/10.3390/rs4051208
- [37] Eldosouky AM, Abdelkareem M, Elkhateeb SO, Journal of African Earth Sciences Integration of remote sensing and aeromagnetic data for mapping structural features and hydrothermal alteration zones in Wadi Allagi area, South Eastern Desert of Egypt. J African Earth Sci, 2017, 130, 28-37, http://dx.doi.org/10.1016/j. jafrearsci.2017.03.006
- [38] Hassan SM, Sadek MF, Journal of African Earth Sciences Geological mapping and spectral based classification of basement rocks using remote sensing data analysis: The Korbiai-Gerf nappe complex, South Eastern Desert, Egypt. J African Earth Sci, 2017, 134, 404-18, http://dx.doi.org/10.1016/j.jafrearsci.2017.07.006
- [39] Liu H, Hong Z, Zhang J, Niu H, Li S, Long L, Sedimentary characteristics and seismic geomorphology of gravity-flow channels in a rift basin: Oligocene Shahejie Formation, Qinan Slope, Huanghua Depression of Bohai Bay Basin, China. Mar Pet Geol, 2014, , 1-19, http://dx.doi.org/10.1016/j.marpetgeo.2016.02.
- [40] Acharya T, Lee D, Yang I, Lee J, Identification of Water Bodies in a Landsat 8 OLI Image Using a J48 Decision Tree. Sensors, 2016, 16 (7), 1075, http://dx.doi.org/10.3390/s16071075
- [41] Mwaniki M, Moeller M, Schellmann G, A comparison of Landsat 8 (OLI) and Landsat 7 (ETM+) in mapping geology and visualising lineaments: A case study of central region Kenya. 2015, XL (May),
- [42] Kamel M, Youssef M, Hassan M, Bagash F, Utilization of ETM + Landsat data in geologic mapping of wadi Ghadir-Gabal Zabara area, Central Eastern Desert, Egypt. Egypt J Remote Sens Sp Sci, 2016, 19 (2), 343-60, http://dx.doi.org/10.1016/j.ejrs.2016.06. 003
- [43] Takodjou Wambo JD, Ganno S, Djonthu Lahe YS, Kouankap Nono GD, Fossi DH, Tchouatcha MS, et al., Geostatistical and GIS analysis of the spatial variability of alluvial gold content in Ngoura-Colomines area, Eastern Cameroon: Implications for the exploration of primary gold deposit. J African Earth Sci, 2018, 142, 138-57, http://dx.doi.org/10.1016/j.jafrearsci.2018.03.015
- [44] Binam Mandeng EP, Bondjè Bidjeck LM, Takodjou Wambo JD, Taku A, Bineli Betsi T, Solange Ipan A, et al., Lithologic and structural mapping of the Abiete-Toko gold district in southern Cameroon, using Landsat 7 ETM+/SRTM. Comptes Rendus Geosci, 2018, 350 (3), 130-40, http://dx.doi.org/10.1016/j.crte. 2017.11.003
- [45] Pour AB, Park Y, Park T-YS, Hong JK, Hashim M, Woo J, et al., Regional geology mapping using satellite-based remote sensing approach in Northern Victoria Land, Antarctica. Polar Sci, 2018, 16, 23-46, http://dx.doi.org/10.1016/j.polar.2018.02.004
- [46] Roy DP, Wulder MA, Loveland TR, C.E. W, Allen RG, Anderson MC, et al., Landsat-8: Science and product vision for terrestrial global change research. Remote Sens Environ, 2014, 145, 154-72, http://dx.doi.org/10.1016/j.rse.2014.02.001

- [47] Mwaniki MW, Matthias MS, Schellmann G, Application of Remote Sensing Technologies to Map the Structural Geology of Central Region of Kenya. IEEE J Sel Top Appl Earth Obs Remote Sens, 2015, 8 (4), 1855–67, http://dx.doi.org/10.1109/jstars.2015.2395094
- [48] Holden CE, Woodcock CE, An analysis of Landsat 7 and Landsat 8 underflight data and the implications for time series investigations. Remote Sens Environ, 2016, 185, 16–36, http://dx.doi.org/10.1016/j.rse.2016.02.052
- [49] Adams JB, Filice AL, Spectral reflectance 0.4 to 2.0 microns of silicate rock powders. J Geophys Res, 1967, 72 (22), 5705–15, http://dx.doi.org/10.1029/jz072i022p05705
- [50] Kariuki PC, Woldai T, Van Der Meer F, Effectiveness of spectroscopy in identification of swelling indicator clay minerals. Int J Remote Sens, 2004, 25 (2), 455-69, http://dx.doi.org/10.1080/0143116031000084314
- [51] Gad S, Kusky T, Lithological mapping in the Eastern Desert of Egypt, the Barramiya area, using Landsat thematic mapper (TM). J African Earth Sci, 2006, 44 (2), 196–202, http://dx.doi.org/10. 1016/j.jafrearsci.2005.10.014
- [52] Ciampalini A, Garfagnoli F, Antonielli B, Del C, Moretti S, Ciampalini A, et al., Photo-lithological map of the southern flank of the Tindouf Basin (Western Sahara). 2012, 5647,
- [53] Abdelmalik. KW and Ali MA. Abd-Allah, Integration of remote sensing technique and field data in geologic mapping of an ophiolitic suture zone in western Arabian Shield. J African Earth Sci, 2018, 146, 180-190.
- [54] Bishta A, Lithologic Discrimination Using Selective Image Processing Technique of Landsat 7 Data, Um Bogma Environs West-central Sinai, Egypt. J King Abdulaziz Univ Sci, 2009, 20 (1), 193–213, http://dx.doi.org/10.4197/ear.20-1.10
- [55] Ali EA, El Khidir SO, Babikir IAA, Abdelrahman ME, Landsat ETM+7 Digital Image Processing Techniques for Lithological and Structural Lineament Enhancement: Case Study Around Abidiya Area, Sudan. Open Remote Sens J, 2012, 5 (1), 83-9, http://dx.doi.org/10.2174/1875413901205010083

- [56] Madani A, Assessment and Evaluation of Band Ratios, Brovey and HSV Techniques for Lithologic Discrimination and Mapping Using Landsat ETM<sup>+</sup> and SPOT-5 Data. Int J Geosci, 2014, 05 (01), 5–11, http://dx.doi.org/10.4236/ijg. 2014.51002
- [57] Corumluoglu O, Vural A, Asri I, Determination of Kula basalts (geosite) in Turkey using remote sensing techniques. Arab J Geosci, 2015, 8 (11), 10105–17, http://dx.doi.org/10.1007/s12517-015-1914-4
- [58] Xu C, Dai F, Xu X, Lee YH, GIS-based support vector machine modeling of earthquake-triggered landslide susceptibility in the Jianjiang River watershed, China. Geomorphology, 2012, 145– 146, 70–80, http://dx.doi.org/10.1016/j.geomorph.2011.12.040
- [59] Pham BT, Tien Bui D, Pourghasemi HR, Indra P, Dholakia MB, Land-slide susceptibility assesssment in the Uttarakhand area (India) using GIS: a comparison study of prediction capability of naïve bayes, multilayer perceptron neural networks, and functional trees methods. Theor Appl Climatol, 2015, 128 (1–2), 255–73, http://dx.doi.org/10.1007/s00704-015-1702-9
- [60] Richards JA, Jia X, Remote Sensing Digital Image Analysis [Internet]. Springer Berlin Heidelberg; 1999., http://dx.doi.org/10.1007/978-3-662-03978-6
- [61] Chen X, Warner TA, Campagna DJ, Integrating visible, near-infrared and short-wave infrared hyperspectral and multispectral thermal imagery for geological mapping at Cuprite, Nevada. Remote Sens Environ, 2007, 110 (3), 344–56, http://dx.doi.org/10.1016/j.rse.2007.03.015
- [62] Ge W, Cheng Q, Tang Y, Jing L, Gao C, Lithological Classification Using Sentinel-2A Data in the Shibanjing Ophiolite Complex in Inner Mongolia, China. Remote Sens, 2018, 10 (4), 638, http://dx.doi.org/10.3390/rs10040638
- [63] Mondal S, Maiti R, Landslide Susceptibility Analysis of Shiv-Khola Watershed, Darjiling: A Remote Sensing & Disamp; GIS Based Analytical Hierarchy Process (AHP). J Indian Soc Remote Sens, 2012, 40 (3), 483–96, http://link.springer.com/10.1007/s12524-011-0160-9